JOURNAL OF MATERIALS SCIENCE 29 (1994) 2903–2910

Kinetics and thermodynamics of intracrystalline Fe–Ga distribution in $Y_3(Fe, Ga)_5O_{12}$

R. NITSCHE*, G. TIPPELT, G. AMTHAUER
Institut für Mineralogie, 5020 Salzburg, Austria

Garnets of composition $Y_3Fe_{5-x}Ga_xO_{12}$, with $x = 0$–5, were synthesized from oxides. Samples with various Ga content were annealed at temperatures between 700–1290 °C; the heating duration varied between 90 s and 1350 h. Cation distribution was measured by Mössbauer spectroscopy at room temperature. The standard free energy change for the exchange reaction $Fe^{3+}(tet) + Ga^{3+}(oct) \leftrightarrow Fe^{3+}(oct) + Ga^{3+}(tet)$ is about 20 kJ mol^{-1}, and decreases slightly with increasing Fe content. The specific rate constants for the ordering process were determined according to the Mueller model for order–disorder kinetics. The activation energies for the ordering process between 200–250 kJ mol^{-1} were calculated from the temperature dependence of the specific rate constants.

1. Introduction

Synthetic garnets of composition $Y_3Fe_2Fe_3O_{12}$ have been known for more than 35 years [1, 2]. Most of the industrial applications are based on their excellent ferrimagnetic properties. The garnet structure consists of a framework of three different oxygen co-ordination polyhedra: a triangular dodecahedra, an octahedra and a tetrahedra [3]. In $Y_3Fe_{5-x}Ga_xO_{12}$ garnets the dodecahedral site is occupied by Y^{3+}, while Fe^{3+} and Ga^{3+} are distributed over the octahedral and tetrahedral sites. Physical properties, e.g. magnetization can be adjusted by cation substitution, for example by substitution of magnetic Fe^{3+} in the garnet structure with diamagnetic Ga^{3+} or Al^{3+}. Sort, amount and cation distribution on crystallographic sites determine the resulting properties. Temperature dependence of the cation distribution is also an important factor.

Several authors investigated intracrystalline cation exchange in Ga-substituted yttrium iron garnets (YIGG) with different methods: paramagnetic resonance [4], nuclear resonance [5], X-ray and neutron diffraction [6], magnetization measurements [7–12] and Mössbauer spectroscopy [13, 14]. Röschmann [15] investigated kinetics of the ordering process in $Y_3Fe_{5-x}Ga_xO_{12}$ with $x < 1$ by magnetization measurements using single crystals. Here, Fe^{3+} and Ga^{3+} distribution is determined in the garnet structure by Mössbauer spectroscopy, and the specific rate constant and the standard free energy change are calculated. Activation energy for the ordering process is calculated from the temperature dependence of the specific rate constants.

2. Experimental details

Garnets of composition $Y_3Fe_{5-x}Ga_xO_{12}$, with $x = 0, 1, 2, 3, 4, 5$, were synthesized by the following procedure. Stoichiometric mixtures of oxides (Y_2O_3, Fe_2O_3, Ga_2O_3) were carefully ground in an agate mortar and pressed into pellets. The mixtures were annealed in four steps from 1100 to 1300 °C for some days, carefully regrinding the reaction products and pressing them into tablets after each step. The final reaction products were quenched in air. Each sample was analysed by optical microscopy and X-ray diffraction to control homogeneity and composition. Diffraction patterns were measured using an automatic diffractometer (Siemens D 500) with CuK_α radiation ($\lambda = 0.15406$ nm, 40 kV, 30 mA) between 10° and 95°, with a 0.01° (2θ) step size and a 6 s measure time per step. Calculation of the lattice constants was done by PC implementation of the algorithm of Appleman and Evans [16]. Pure silicon was used as an internal standard.

Samples of composition $Y_3Fe_5O_{12}$ and $Y_3Ga_5O_{12}$ were only used for calculation of the lattice constants. Cation distribution was investigated for $Y_3Fe_{5-x}Ga_xO_{12}$, with $x = 1, 2, 3, 4$. Finally, $Y_3Fe_3Ga_2O_{12}$ and $Y_3Fe_1Ga_4O_{12}$ were chosen for the kinetic experiments. For the kinetic experiments, samples of approximately 30 mg were sealed into platinum tubes and suspended from a platinum wire in a vertical tube furnace. After annealing at temperatures between 700–1290 °C, for times between 90 s and 56 days (Table I) the wire was cut and samples were quenched in an ice water bath below the furnace.

Mössbauer spectra were measured using a velocity generator operated at constant acceleration (v_{max} = 4 mm s^{-1} for the non-magnetic and 12 mm s^{-1} for the magnetic spectra) with symmetric triangular wave form. Spectra were recorded at room temperature, or liquid nitrogen temperature, with a 25 or 50 mCi $^{57}Co/Rh$ source of 6 mm diameter. Absorbers had diameters of 10 mm and densities of 1.25 or 2.5 mg

* *Present address*: Technische Hochschule Darmstadt, Fachbereich Materialwissenschaft, 64295 Darmstadt, Germany.

TABLE I Fe^{3+} site occupancies, X, and areas, A, in % ($\pm$ 1%) for $Y_3Fe_1Ga_4O_{12}$ and $Y_3Fe_3Ga_2O_{12}$ at various temperatures: (at) annealing time, (tet) tetrahedron, (oct) octahedron

(a)

	$Y_3Fe_1Ga_4O_{12}$					$Y_3Fe_3Ga_2O_{12}$			
	Fe^{3+}(tet)		Fe^{3+}(oct)			Fe^{3+}(tet)		Fe^{3+}(oct)	
at (h)	A (%)	X	A (%)	X	at (h)	A (%)	X	A (%)	X
Temperature 700 °C									
50[a]	28.98	0.097	71.02	0.355	–	–	–	–	–
120	25.12	0.084	74.88	0.374	–	–	–	–	–
170[a]	24.67	0.082	75.33	0.377	–	–	–	–	–
210[a]	24.89	0.083	75.11	0.376	–	–	–	–	–
265[a]	23.46	0.078	76.54	0.383	–	–	–	–	–
315	21.83	0.073	78.17	0.391	–	–	–	–	–
507	21.83	0.073	78.17	0.391	–	–	–	–	–
507[a]	22.07	0.074	77.93	0.390	–	–	–	–	–
793[a]	19.61	0.065	80.39	0.402	–	–	–	–	–
1033[a]	19.97	0.067	80.03	0.400	–	–	–	–	–
1350[a]	20.82	0.069	79.18	0.396	–	–	–	–	–
Temperature 800 °C									
3	28.03	0.093	71.93	0.360	3	47.51	0.475	52.49	0.787
6.5[a]	25.24	0.084	74.76	0.374	3[a]	47.03	0.470	52.97	0.795
10	24.04	0.080	75.96	0.380	20	44.89	0.449	55.11	0.827
20	22.95	0.073	77.05	0.391	50	42.46	0.425	57.54	0.863
20[a]	21.89	0.077	78.11	0.385	124	42.22	0.422	57.78	0.867
30	20.30	0.068	79.70	0.399	167	42.20	0.422	57.81	0.867
48	20.88	0.070	79.12	0.396	–	–	–	–	–
80	20.85	0.070	79.15	0.396	–	–	–	–	–
115[a]	19.66	0.066	80.34	0.402	–	–	–	–	–
120	19.61	0.065	80.39	0.402	–	–	–	–	–
Temperature 900 °C									
0.5[a]	28.49	0.095	71.51	0.358	2	45.97	0.460	54.14	0.812
0.75[a]	27.07	0.090	72.93	0.365	4	44.52	0.445	55.47	0.832
1	24.38	0.081	75.62	0.378	8	42.70	0.427	57.30	0.860
2	22.36	0.075	77.64	0.388	16	42.45	0.425	57.56	0.863
8	21.91	0.073	78.09	0.390	25	42.89	0.429	57.11	0.857
16	21.80	0.073	78.20	0.391	40	43.59	0.436	56.41	0.846
16[a]	21.38	0.071	78.62	0.393	40[a]	42.92	0.429	57.08	0.856
25	21.84	0.073	78.16	0.391	60	42.66	0.427	57.34	0.860
40	20.88	0.070	79.12	0.396	–	–	–	–	–
40[a]	20.68	0.069	79.32	0.397	–	–	–	–	–
65	22.46	0.075	77.54	0.388	–	–	–	–	–
72	22.70	0.076	77.30	0.386	–	–	–	–	–

(b)

	$Y_3Fe_1Ga_4O_{12}$					$Y_3Fe_3Ga_2O_{12}$			
	Fe^{3+}(tet)		Fe^{3+}(oct)			Fe^{3+}(tet)		Fe^{3+}(oct)	
at (min)	A (%)	X	A (%)	X	at (min)	A (%)	X	A (%)	X
Temperature 1000 °C									
2.5[a]	30.11	0.100	69.89	0.350	30	46.52	0.465	53.48	0.802
5	27.67	0.092	72.33	0.362	60	43.83	0.438	56.17	0.843
15	25.37	0.085	74.63	0.373	240	44.41	0.444	55.59	0.834
30	24.23	0.081	75.77	0.379	300	44.76	0.448	55.24	0.829
60	24.08	0.080	75.92	0.380	360	42.57	0.426	57.43	0.861
180	23.92	0.080	76.08	0.380	600	43.22	0.432	56.78	0.852
600[a]	24.40	0.081	75.60	0.378	1080	44.84	0.448	55.17	0.828
–	–	–	–	–	1200	43.88	0.439	56.12	0.842
–	–	–	–	–	1800	43.16	0.432	56.85	0.853
Temperature 1100 °C									
1.5[a]	30.32	0.101	69.68	0.348	30	46.24	0.462	53.76	0.806
3[a]	28.55	0.095	71.45	0.357	60	45.67	0.457	54.33	0.815
3[a]	28.42	0.095	71.58	0.358	300	45.46	0.455	54.54	0.818
5	27.49	0.092	72.51	0.363	540	46.37	0.464	53.63	0.804
8	27.97	0.093	72.03	0.360	–	–	–	–	–
9[a]	26.49	0.088	73.51	0.368	–	–	–	–	–
10[a]	26.93	0.090	73.07	0.365	–	–	–	–	–
10[a]	27.72	0.092	72.28	0.361	–	–	–	–	–
13[a]	27.05	0.090	72.95	0.365	–	–	–	–	–
60[a]	26.23	0.087	73.77	0.369	–	–	–	–	–
1200	26.13	0.087	73.87	0.369	–	–	–	–	–

TABLE I (b) Continued

	$Y_3Fe_1Ga_4O_{12}$					$Y_3Fe_3Ga_2O_{12}$			
	Fe^{3+}(tet)		Fe^{3+}(oct)			Fe^{3+}(tet)		Fe^{3+}(oct)	
at (min)	A (%)	X	A (%)	X	at (min)	A (%)	X	A (%)	X
Temperature 1200 °C									
1320	28.70	0.096	71.30	0.357	15	47.22	0.472	52.78	0.792
–	–	–	–	–	30	46.56	0.466	53.44	0.802
–	–	–	–	–	60	46.84	0.468	53.16	0.797
–	–	–	–	–	180	46.70	0.467	53.30	0.780
Temperature 1290 °C									
1440	30.59	0.102	69.41	0.347	–	–	–	–	–
Temperature 1300 °C									
6840	30.88	0.103	69.12	0.346	17400	47.86	0.479	52.14	0.782
6840	31.28	0.104	68.72	0.344	17400	46.55	0.466	53.45	0.802

[a] Measured with a 50 mCi source.

Fe cm^{-2}. The distance between absorber and source was about 15 cm. A scintillation counter with an Tl-doped natrium iodide crystal was used as a detector. Spectra were recorded by a multichannel analyser (1024 channels) and the two symmetric parts (512 channels each) were folded before evaluation. The counting rate was approximately 900 000 counts per channel. Spectra were fitted assuming a Lorenzian shape for the lines using a distance least squares fitting program. The velocity scale was calibrated with an α-Fe foil.

3. Results

3.1. X-ray diffraction

Synthesis progress was controlled by X-ray diffraction patterns. After annealing the oxides for several hours at 1100 °C, garnet is the dominant phase; but residues of all oxides and another phase, $YFeO_3$ (yttrium orthoferrite), can also be detected. Continuing synthesis at 1300 °C, the amount of garnet is continually increasing at the cost of $YFeO_3$ and the oxides, until formation of the garnet phase is completed. The values of the lattice constants are in good agreement with those of many other authors [6, 7, 9, 14, 17–28]. Fig. 1 shows a distinct non-linear decrease with increasing Ga content. This non-ideal mixing of the component end members, $Y_3Fe_5O_{12}$ and $Y_3Ga_5O_{12}$, corresponds with an ideal mixing on the individual sites [29], which was assumed as a simplification of the calculation of the rate constants.

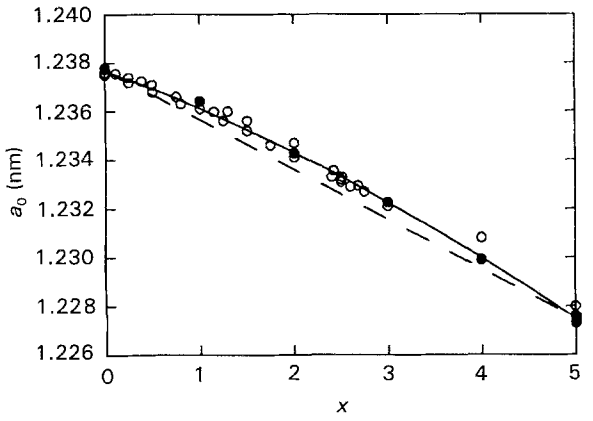

Figure 1 Lattice constants of $Y_3Fe_{5-x}Ga_xO_{12}$. (○) data from literature, (●) data from this study, (——) fit of data, (– –) ideal mixture.

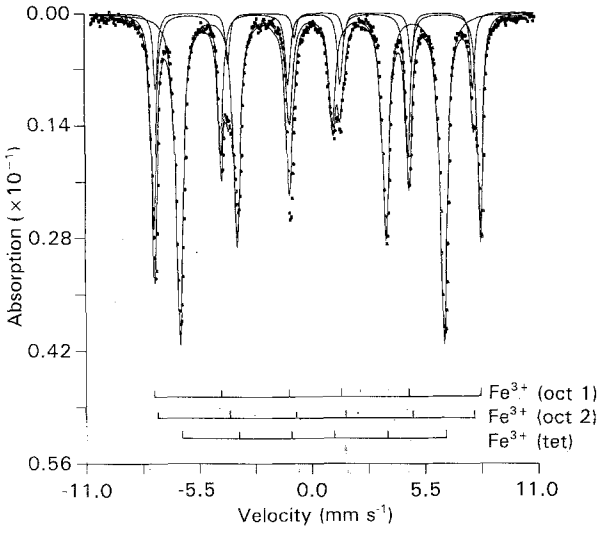

Figure 2 Mössbauer spectrum of $Y_3Fe_5O_{12}$ synthesised at 1300 °C and 100 Pa.

3.2. Mössbauer spectroscopy

After annealing and quenching all samples were investigated by Mössbauer spectroscopy. Compositions of the system $Y_3Fe_{1-x}Ga_xO_{12}$ with a Ga content less than about $x = 1.8$ are ferrimagnetic at room temperature. The absorption line is split in a sextet, because of magnetic hyperfine interaction. In pure $Y_3Fe_5O_{12}$, two of the five Fe^{3+} ions occupy the octahedral sites, while the tetrahedral sites are occupied by three Fe^{3+} ions. Interpretation of the sextets, with only one sort of ion distributed among two crystallographic sites to varying extents, is relatively easy. This spectrum can be evaluated with two or three sextets. The sextet with the bigger absorption is assigned to the tetrahedral site, the sextet with less absorption to the octahedral site (Fig. 2). In addition, the octahedron sextet can be

split in two sextets, corresponding to two nearly identical octahedra. There are two different octahedra, because of two possible angles between the axis of the nuclear electric field gradient and the magnetic field [30]. Mössbauer spectra of $Y_3Fe_5O_{12}$ were taken at room temperature and liquid nitrogen temperature. Mössbauer parameters are listed in Table II.

Substitution of one paramagnetic Fe^{3+} ion by a diamagnetic Ga^{3+} ion leads to a quite different spectrum (Fig. 3). The full width at half maximum (FWHM) for the sextets increases extremely, and in the centre of the spectrum paramagnetic doublets can be observed (Table II). This phenomenon was investigated by Coey [31]. However, this type of spectra is too complicated for kinetic calculations. Mössbauer parameters in this spectrum can be varied over a large range without influencing the goodness of fit. Hence, calculated values for site occupancies from the distance least square fit are not accurate enough for kinetic calculations. *In situ* high temperature measurements, above the Curie temperature, would be a solution to this problem.

Compositions with $x > 1.8$ have a Curie temperature less than room temperature. Samples of these compositions have paramagnetic properties at room temperature [32]. This leads to a second type of spectra that consists of two doublets. Spectra obtained on samples of the composition $YFe_{5-x}Ga_xO_{12}$, with $x = 2, 3, 4$, show three absorption maxima at room temperature which can be fitted with two doublets (Figs 4 and 5). The doublet with the smaller quadrupole split and the larger isomer shift is related to the octahedral site. The doublet with the larger quadrupole split and the smaller isomer shift is related to the tetrahedral site. The Fe^{3+} content on the octahedral site increases with annealing time. Observed data and

TABLE II Mössbauer parameter for $Y_3Fe_5O_{12}$ and $Y_3Fe_4Ga_1O_{12}$ synthesised at 1300 °C and 100 Pa: (IS) isomer shift related to α-Fe, (Γ) full width at half maximum, (QS) quadrupole splitting, (Hm) magnetic field strength, (Θ) angle between Hm and V_{ZZ}, (A) areas in % tetrahedral or octahedral site, (χ^2) goodness of fit, (rt) room temperature, (lnt) liquid nitrogen temperature, (oct) octahedron, (tet) tetrahedron, (dbl) doublet

Site	IS ($mm\,s^{-1}$)	Γ ($mm\,s^{-1}$)	QS ($mm\,s^{-1}$)	Hm (T)	Θ (° deg)	A (%)
$Y_3Fe_5O_{12}$ at rt (χ^2 = 3.160)						
Oct 1	0.356	0.296	1.302	49.23	48.8	29.29
Oct 2	0.427	0.294	1.264	47.92	76.2	8.89
Tet	0.149	0.410	1.058	39.40	54.9	61.82
$Y_3Fe_5O_{12}$ at lnt (χ^2 = 0.730)						
Oct 1	0.479	0.266	1.089	54.73	35.1	28.86
Oct 2	0.473	0.254	1.073	53.82	73.4	10.13
Tet	0.242	0.356	0.975	46.63	54.6	61.02
$Y_3Fe_4GaO_{12}$ at rt (χ^2 = 3.036)						
Oct	0.166	0.866	0.752	34.82	53.8	33.02
Tet	0.411	0.860	0.517	41.64	57.3	66.98
Dbl 1	0.283	0.166	2.069	–	–	2.31
Dbl 2	0.238	0.206	1.678	–	–	1.65

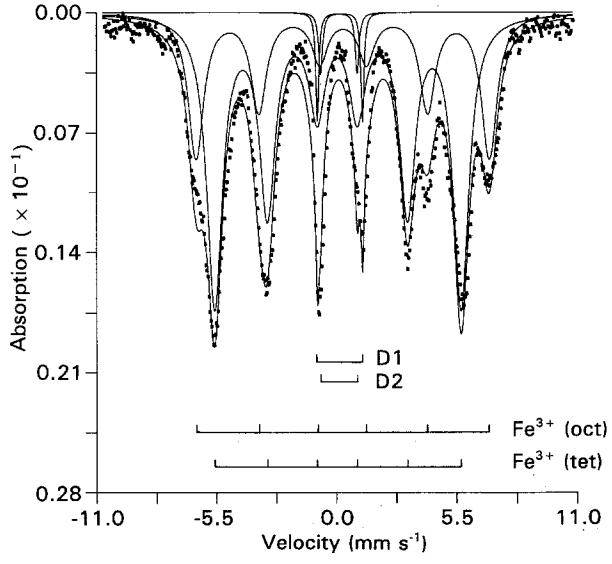

Figure 3 Mössbauer spectrum of $Y_3Fe_4Ga_1O_{12}$ synthesised at 1300 °C and 100 Pa.

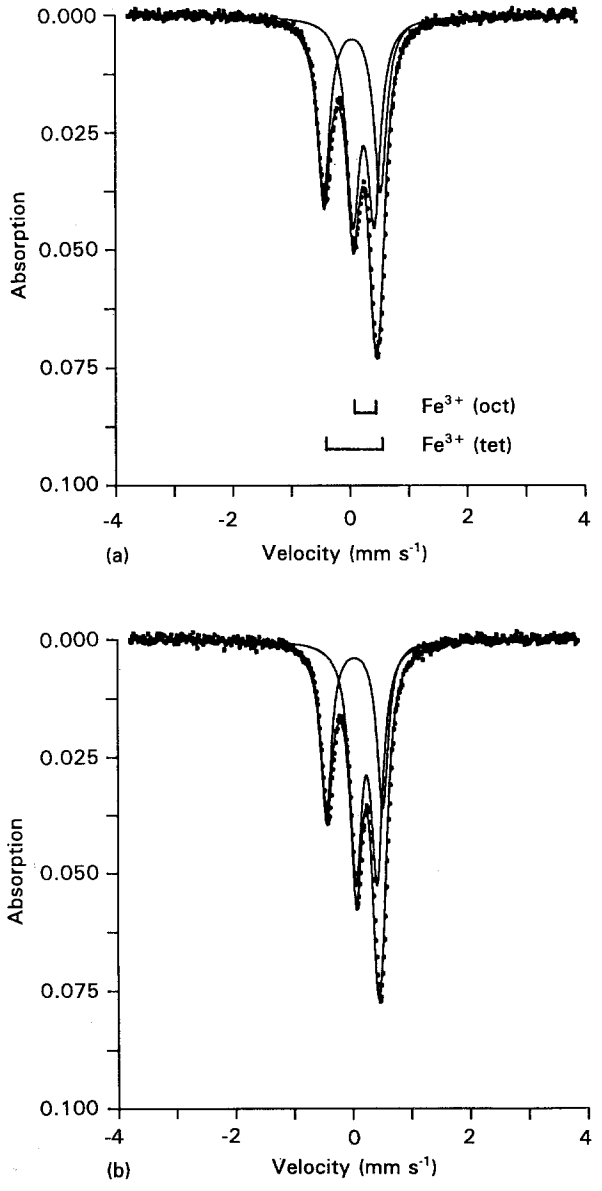

Figure 4 Mössbauer spectra of $Y_3Fe_3Ga_2O_{12}$ (a) synthesised at 1300 °C and 100 Pa, and (b) annealed for 167 h at 800 °C and 100 Pa.

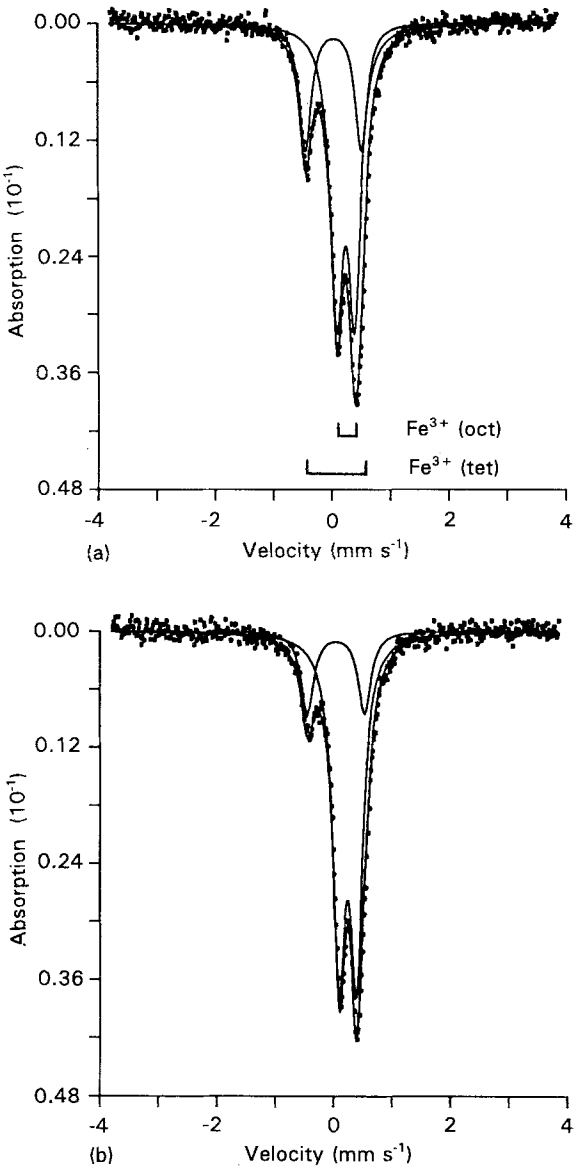

Figure 5 Mössbauer spectra of $Y_3Fe_1Ga_4O_{12}$ (a) synthesised at 1300 °C and 100 Pa, and (b) annealed for 1350 h at 700 °C and 100 Pa.

TABLE III Mössbauer parameter for $Y_3Fe_3Ga_2O_{12}$, $Y_3Fe_2Ga_3O_{12}$ and $Y_3Fe_1Ga_4O_{12}$ synthesised at 1300 °C and 100 Pa: (IS) isomer shift related to α-Fe, (Γ) full width at half maximum, (QS) quadrupole splitting, (χ^2) goodness of fit

	Site	IS ($mm\,s^{-1}$)	QS ($mm\,s^{-1}$)	Γ ($mm\,s^{-1}$)
$Y_3Fe_3Ga_2O_{12}$	tetrahedron	0.151	0.955	0.262
χ^2 = 0.536	octahedron	0.350	0.352	0.260
$Y_3Fe_2Ga_3O_{12}$	tetrahedron	0.145	0.931	0.232
χ^2 = 0.380	octahedron	0.342	0.319	0.232
$Y_3Fe_1Ga_4O_{12}$	tetrahedron	0.146	0.955	0.252
χ^2 = 0.370	octahedron	0.346	0.297	0.262

calculated spectra are in good agreement. Therefore, this kind of spectra can be used for kinetic calculations. The site occupancies were calculated under the assumption that the recoil free fractions of Fe^{3+} at different sites are the same [14]. Mössbauer parameters of the synthesis products are listed in Table III.

Isomer shift shows almost constant values, whereas quadrupole splitting varies significantly. The reason for this variation is probably the use of two different ^{57}Co sources (25 mCi and 50 mCi). The values for the quadrupole splitting decrease by using the stronger source (Table IV). Fig. 6 shows isomer shift and quadrupole splitting dependent on the ^{57}Co source. There are obviously two concentrations for the values of quadrupole splitting dependent on the ^{57}Co source. Further investigations are necessary to clear up this relationship.

4. Discussion

The distribution of Fe^{3+} and Ga^{3+} among tetrahedral and octahedral sites is not random. Fe^{3+} ions show a significant preference for the octahedral site. This preference decreases with increasing temperature (Table I). Time and temperature dependence of the cation ordering are used for kinetic calculations. Cation ordering among two crystallographic sites can be described by the following equation

$$Fe^{3+}(tet) + Ga^{3+}(oct) \leftrightarrow Fe^{3+}(oct) + Ga^{3+}(tet) \quad (1)$$

Assuming ideal solid solution of Fe^{3+} and Ga^{3+} among tetrahedral and octahedral sites, the specific rate constant C_0k and the distribution coefficient K_D

TABLE IV Quadrupole splitting ($mm\,s^{-1}$) for $Y_3Fe_1Ga_4O_{12}$ dependent on the ^{57}Co source

	25 mCi	50 mCi
Tetrahedron		
Minimum	0.966	0.947
Mean	0.984	0.959
Maximum	0.996	0.970
Octahedron		
Minimum	0.299	0.290
Mean	0.309	0.298
Maximum	0.315	0.306

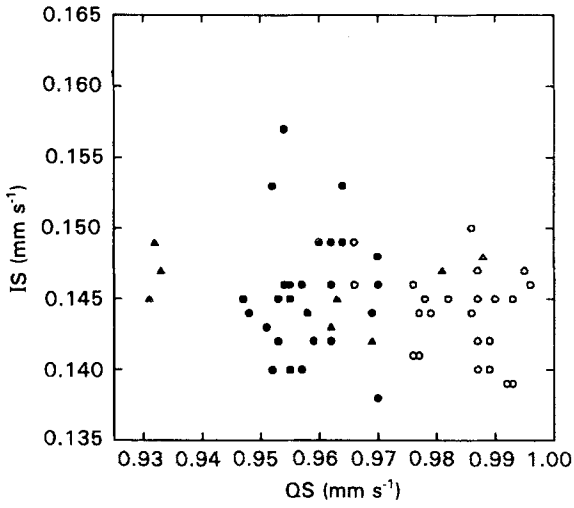

Figure 6 Variation of isomer shift (IS) and quadrupole splitting (QS) dependent on the use of different ^{57}Co sources: (○) $Y_3Fe_1Ga_4O_{12}$, 25 mCi; (●) $Y_3Fe_1Ga_4O_{12}$, 50 mCi; (△) $Y_3Fe_2Ga_3O_{12}$, 25 mCi; (▲) $Y_3Fe_2Ga_3O_{12}$, 50 mCi.

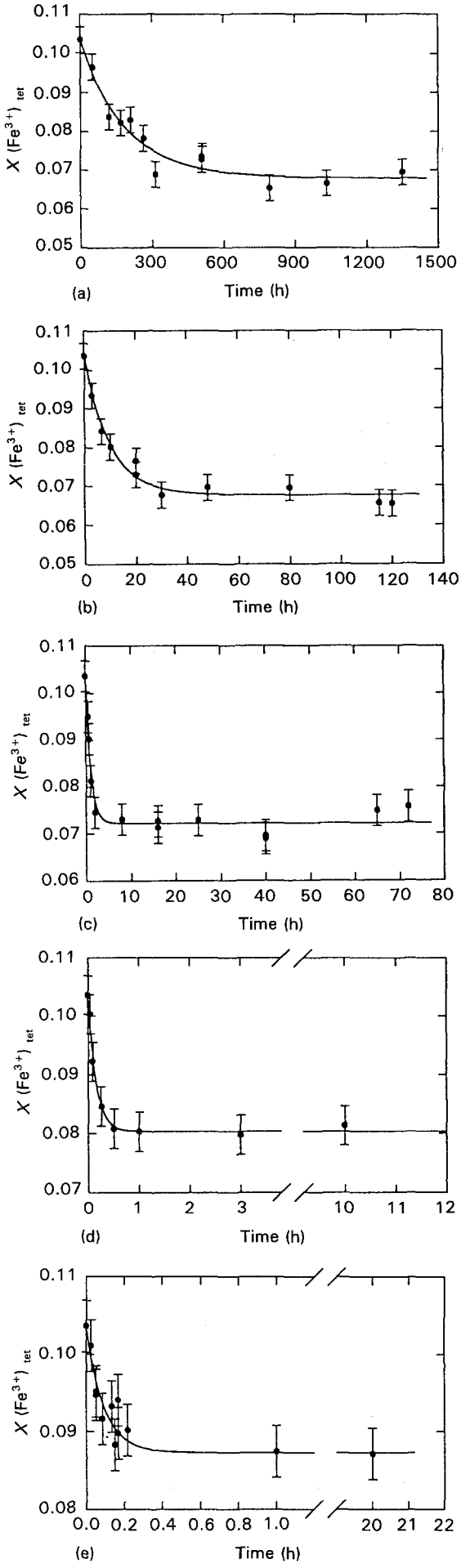

Figure 7 Ordering experiments at various temperatures and 100 Pa on $Y_3Fe_1Ga_4O_{12}$, (a) 700 °C, (b) 800 °C, (c) 900 °C, (d) 1000 °C and (e) 1100 °C.

can be calculated according to Mueller's kinetic model [33–35]. For these calculations the Mueller equation was rearranged to the following form

$$X_i^A(t) = \frac{[\exp(-C_0k\Delta tA)](-bB-AB)+b-A}{[\exp(-C_0k\Delta tA)](2aB)-2a} \quad (2)$$

with: $A = (b^2 - 4ac)^{1/2}$

$B = (2aX_iA_0 + b - A)/(2aX_iA_0 + b + A)$

$a = p(1 - K_D^{-1})$

$b = q - X_i + K_D^{-1}(X_i + p)$

$c = -K_D^{-1}X_i$

$p = C_A/C_0$

$q = C_B/C_0$

$C_0 = C_A + C_B$

where X_i^A is the mole fraction for tetrahedral site, X_i the mole fraction for both sites, C_A the molar concentration of tetrahedral sites available for the exchange, C_B the molar concentration of octahedral sites available for the exchange, k the specific rate constant, K_D the distribution coefficient, and t is time.

Fig. 7 shows the experimental data and the calculated fit of the Fe^{3+} tetrahedron occupancy, dependent on time and temperature, for $Y_3Fe_1Ga_4O_{12}$ at temperatures between 700–1100 °C and 100 Pa. Some heating experiments have been done twice, so the accuracy of the site occupancy data is estimated within ± 1%. Calculated values of the specific rate constants and the distribution coefficients are listed in Table V. The distribution coefficients for $Y_3Fe_1Ga_4O_{12}$ at 700 and 800 °C are very similar. Thus, it seems that maximum order for this composition is reached between 700–800 °C. For a definite statement, additional long time annealing experiments at low temperatures have to be carried out. The concentration of oxygen vacancies influences diffusion

TABLE V Fe^{3+} tetrahedral site occupancies, distribution coefficients, K_D, specific rate constants, C_0k, and standard free energy change, ΔG, for $Y_3Fe_3Ga_2O_{12}$, $Y_3Fe_2Ga_3O_{12}$ and $Y_3Fe_1Ga_4O_{12}$

Temperature (°C)	Fe^{3+} (tet) (%)	K_D	C_0k (h^{-1})	ΔG (kJ mol^{-1})	
800	42.02	9.214	0.0827	− 19.81	
900	42.83	8.041	0.6212	− 20.33	
1000	43.79	6.899	2.8877	− 20.44	$Y_3Fe_3Ga_2O_{12}$
1100	45.84	5.115	6.2470	− 18.63	
1200	46.70	4.550	4.8966	− 18.56	
1300	47.20	4.259	–	− 18.95	
800	57.60	10.402	–	− 20.90	
900	63.28	8.081	–	− 20.38	
1000	68.50	6.488	–	− 19.80	$Y_3Fe_2Ga_3O_{12}$
1100	72.85	5.443	–	− 19.34	
1200	76.05	4.799	–	− 19.21	
1300	79.66	4.178	–	− 18.70	
700	20.38	9.086	0.0136	− 17.86	
800	20.28	9.140	0.2724	− 19.74	
900	21.65	8.280	2.4574	− 20.62	
1000	24.08	7.009	16.5436	− 20.61	$Y_3Fe_1Ga_4O_{12}$
1100	26.18	6.118	27.2072	− 20.67	
1200	28.70	5.238	–	− 20.28	
1290	30.59	4.681	–	− 20.06	
1300	31.08	4.549	–	− 19.82	

and consequently, kinetic data. Therefore, the kind of atmosphere is decisive for kinetic experiments. Thus, in another atmosphere, different results are expected. On the other hand, changes of the concentration of oxygen vacancies during heating experiments can be ignored [11].

Activation energy, E_A, for the intracrystalline ordering process can be calculated using the Arrhenius equation

$$k = k^* \exp(-E_A/RT) \quad (3)$$

where E_A is the activation energy; R is the gas constant and T is the temperature (k).

Fig. 8 shows the natural logarithm of the specific rate constant, C_0k, as a function of the reciprocal temperature for $Y_3Fe_3Ga_2O_{12}$ and $Y_3Fe_1Ga_4O_{12}$. Between 700–1000 °C these two parameters are linear dependent. Thus, it can be supposed that the exchange mechanism is the same within this temperature range. The deviation at higher temperatures is due to re-ordering because of too low a quenching rate rather than to a different exchange mechanism. However, activation energies have been calculated using only specific rate constants up to 1000 °C. An activation energy of 243 kJ mol^{-1} is found for the ordering process in $Y_3Fe_1Ga_4O_{12}$. The activation energy is 202 kJ mol^{-1} for the ordering process in $Y_3Fe_3Ga_2O_{12}$ in the temperature range 800–1000 °C.

Distribution coefficient data are used to calculate the standard free energy change, ΔG_{ex}, of the exchange reaction during the ordering process (Equation 4)

$$\Delta G_{ex} = -RT \ln K_D \quad (4)$$

The calculated amount of Fe^{3+} on the tetrahedral site, distribution coefficient and standard free energy change are listed in Table V. Negative values for ΔG_{ex} illustrate the preference of Fe^{3+} for the octahedral site. ΔG_{ex} increases very slightly with decreasing temperature. Similar results have been reported for other compounds [36–38]. Considering average values, ΔG_{ex} is slightly decreasing with decreasing Ga^{3+} content (Table VI). This fact corresponds to the real miscibility of the system $Y_3Fe_{5-x}Ga_xO_{12}$.

According to the equation

$$\Delta G = \Delta H - T\Delta S \quad (5)$$

excess configurational entropy contribution, ΔS, and enthalpy difference between the disordered and ordered state, ΔH, can be calculated. These data are listed in Table VI. As expected the entropy term is very small.

TABLE VI ΔG_{ex}, ΔH_{ex} and ΔS_{ex} of $Y_3Fe_3Ga_2O_{12}$ and $Y_3Fe_1Ga_4O_{12}$ for the ordering process between 800–1000 °C

	ΔG_{ex} (kJ mol^{-1})	ΔH_{ex} (kJ mol^{-1})	ΔS_{ex} (kJ mol^{-1})
$Y_3Fe_3Ga_2O_{12}$	− 20.07	− 16.50	− 3.15
$Y_3Fe_1Ga_4O_{12}$	− 20.26	− 20.72	− 0.34

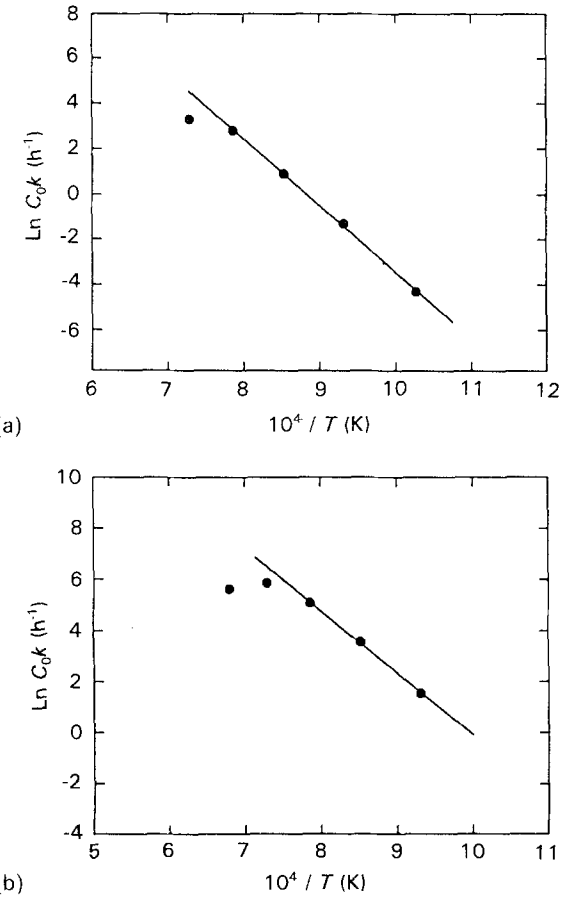

Figure 8 Arrhenius plot for (a) $Y_3Fe_1Ga_4O_{12}$ and (b) $Y_3Fe_3Ga_2O_{12}$.

5. Conclusions

Mössbauer spectra of compositions with paramagnetic properties at room temperature can be used to calculate kinetic and thermodynamic data of ordering or disordering processes. Evaluation of spectra from compositions with ferrimagnetic properties at room temperature is not as definite as necessary to calculate activation energies or specific rate constants. Reliable kinetic data for these compositions can only be determined by *in situ* high temperature measurements above the Curie temperature of the investigated composition.

Quenching is also an important factor for kinetic calculations. At high temperatures (> 1000 °C) re-ordering processes alter the results of ordering experiments. At low temperatures (< 800 °C) the ordering process becomes very slow and perhaps maximum order is already reached. Hence, kinetic data can only be determined in a relatively small temperature range.

References

1. F. BERTAUT and F. FORRAT, *Compt. Rend.* **242** (1956) 382.
2. S. GELLER and M. A. GILLEO, *Acta Cryst.* **10** (1957) 239.
3. S. GELLER, *Z. Kristallographie* **125** (1967) 1.
4. S. GESCHWIND, *Phys. Rev.* **121** (1961) 363.
5. R. L. STREEVER and G. A. URIANO, *ibid.* **139** (1965) A305.
6. P. FISCHER, W. HÄLG, E. STOLL and A. SEGMÜLLER, *Acta Cryst.* **21** (1966) 765.
7. M. A. GILLEO and S. GELLER, *Phys. Rev.* **110** (1958) 73.

8. B. LÜTHI and T. HENNINGSEN, in Proceedings of the International Conference on Magnetism, Nottingham, (Institute of Physics and the Physics Society, London, 1965) 668.
9. S. GELLER, J. A. CAPE, G. P. ESPINOSA and D. H. LESLIE, *Phys. Rev.* **148** (1966) 522.
10. P. GÖRNERT and C. G. D'AMBLY, *Phys. Stat. Sol.* **(a) 29** (1975) 95.
11. P. RÖSCHMANN, *J. Phys. Chem. Solids* **41** (1980) 569.
12. P. RÖSCHMANN and P. HANSEN, *J. Appl. Phys.* **52** (1981) 6257.
13. E. R. CZERLINSKY, *Phys. Stat. Sol.* **34** (1969) 483.
14. G. AMTHAUER, V. GÜNZLER, S. S. HAFNER and D. REINEN, *Z. Kristallographie* **161** (1982) 167.
15. P.RÖSCHMANN, *J. Phys. Chem. Solids* **42** (1981) 337.
16. D. E. APPLEMAN and H. T. EVANS, US Geological Survey, Comp. Contr. 20, US Nat. Techn. Inf. Serv., Doc. PB2-16188. (1973).
17. F. BERTAUT and F. FORRAT, *Compt. Rend.* **244** (1957) 96.
18. G. VILLERS and J. LORIERS, *ibid.* **245** (1957) 2033.
19. S. J. SCHNEIDER, R. S. ROTH and J. L. WARING, *J. Res. Nat. Bur. Stand.* **65A** (1961) 345.
20. G. P. ESPINOSA, *Inorg. Chem.* **3** (1964) 848A.
21. S. GELLER, H. J. WILLIAMS, G. P. ESPINOSA and R. C. SHERWOOD, *Bell. Syst. Tech. J.* **43** (1964) 565.
22. F. EULER and J. A. BRUCE, *Acta Cryst.* **19** (1965) 971.
23. H. J. LEVINSTEIN, E. M. GYORGY and R. C. LeCRAW, *J. Appl. Phys.* **37** (1966) 2197.
24. M. MAREZIO, J. P. REMEIKA and P. D. DERNIER, *Acta Cryst.* **B24** (1968) 1670.
25. E. A. GIESS, B. A. CALHOUN, E. KLOKHOLM, T. R. McGUIRE and L. L. ROSIER, *Mater. Res. Bull.* **6** (1971) 317.
26. G. WINKLER, P. HANSEN and P. HOLST, *Philips Res. Repts* **27** (1972) 151.
27. A. M. VAN DER KRAAN, J. J. VAN LOEF and W. TOLKSDORF, *Phys. Stat. Sol. (a)* **17** (1973) K79.
28. B. STROCKA, P. HOLST and W. TOLKSDORF, *Philips J. Res.* **33** (1978) 186.
29. R. F. MUELLER and S. GHOSE, *Amer. Min.* **55** (1970) 1932.
30. G. A. SAWATZKY, F. VAN DER WOUDE and A. H. MORRISH, *Phys. Rev.* **183** (1969) 383.
31. J. M. D. COEY, *Phys. Rev. B* **6** (1972) 3240.
32. G. WINKLER, "Magnetic Garnets" (Vieweg & Sohn, Braunschweig/Weisbaden, 1981) p. 735.
33. R. F. MUELLER, *J. Phys. Chem. Solids* **28** (1967) 2239.
34. *Idem.*, Mineralogical Society of America, Special Paper **2** (1969) 117.
35. J. GANGULY, in "Advances in Physical Geochemistry", Vol. 2, edited by S. K. Saxena (Springer Verlag, New York, 1982) p. 58.
36. J. R. BESANCON, *Amer. Min.* **66** (1981) 965.
37. F. SEIFERT, *Amer. J. Sci.* **278** (1978) 1323.
38. H. SKOGBY, *Phys. Chem. Min.* **14** (1987) 521.

Received 17 May
and accepted 24 November 1993